catalysts

MDPI

Article

Catalytic Deoxygenation of Hexadecyl Palmitate as a Model Compound of Euglena Oil in H_2 and N_2 Atmospheres

Yanyong Liu *, Megumu Inaba and Koichi Matsuoka

National Institute of Advanced Industrial Science and Technology, AIST Tsukuba West, 16-1 Onogawa, Tsukuba, Ibaraki 305-8569, Japan; mg.inaba@aist.go.jp (M.I.); koichi-matsuoka@aist.go.jp (K.M.)

* Correspondence: yy.ryuu@aist.go.jp; Tel.: +81-29-861-4826

Received: 15 October 2017; Accepted: 5 November 2017; Published: 9 November 2017

Abstract: Hexadecyl palmitate ($C_{15}H_{31}COOC_{16}H_{33}$, used as a model compound for Euglena oil) was deoxygenated to hydrocarbons over various solid catalysts in autoclave reactors. In a H_2 atmosphere, 1 wt.% of Pd/Mg(Al)O catalyst, derived from a hydrotalcite precursor, yielded a $C_{15}H_{31}COOC_{16}H_{33}$ conversion close to 100%, and a C_{10}–C_{16} (aviation fuel range) hydrocarbon yield of 90.2% for the deoxygenation of $C_{15}H_{31}COOC_{16}H_{33}$ at 300 °C for 2 h. In a N_2 atmosphere, 1 wt.% of Pd/Mg(Al)O catalyst yielded a C_{10}–C_{16} hydrocarbon yield of 63.5%, which was much higher than those obtained with Mg(Al)O (15.1%), H-ZSM-5 (8.3%), and 1 wt.% Pd/C (26.2%) for the deoxygenation of $C_{15}H_{31}COOC_{16}H_{33}$ at 300 °C for 2 h. The Pd metal site and the solid base site in Mg(Al)O had a synergetic effect on the deoxygenation of $C_{15}H_{31}COOC_{16}H_{33}$ in N_2 atmosphere over the Pd/Mg(Al)O catalyst. By prolonging the reaction time to 5 h for reaction at 300 °C in N_2 atmosphere, the yield of C_{10}–C_{16} hydrocarbons increased to 80.4% with a $C_{15}H_{31}COOC_{16}H_{33}$ conversion of 99.1% over the 1 wt.% Pd/Mg(Al)O catalyst.

Keywords: hexadecyl palmitate; Euglena oil; deoxygenation; aviation fuel range hydrocarbons; hydrotalcite; Pd catalyst; N_2 atmosphere; H_2 atmosphere

1. Introduction

The production of chemicals and transport fuels from renewable biomass is a sustainable and environment-friendly way to reduce the world's dependence on crude oil. Starch and cellulose in wood can be converted to ethanol by yeast fermentation [1]. Lignin in wood and organic wastes can be converted to motor fuels by a biomass-to-liquid (BTL) process using a syngas platform [2,3]. Vegetable oils can be converted to fatty acid methyl esters (FAME, known as biodiesel) by transesterification with methanol [4]. Recently, the hydrotreatment of vegetable oils to produce hydrocarbon 'drop-in' fuels has attracted global research interest [5–7].

Algae oils have recently become a promising alternative feedstock for vegetable oils because the oil yields from algae are significantly higher than those from any other crop [8–11]. Euglena is a promising algae biomass because it is easily cultivated on a large scale. Most algae produce oils composed of triglycerides and fatty acids [8]. However, Euglena produces an oil wax that contains a mixture of saturated esters with long carbon chains ($C_mH_{2m+1}COOC_nH_{2n+1}$, m = 11–15, n = 12–16) [12,13]. While some studies have been reported on the deoxygenation of triglycerides and fatty acids (vegetable oils and algae oils), very few studies have reported on the deoxygenation of fatty acid esters to date [14].

Metal (NiMo, Pt, etc.)-supported catalysts possess high activities for the deoxygenation of triglycerides and fatty acids in H_2 atmosphere [15–17]. However, the deoxygenation of triglycerides in N_2 atmosphere (without H_2) is an important subject, because H_2 is expensive and may be difficult to obtain in areas of vegetable and algae cultivation. Solid acids and bases have been reported as

catalysts for the deoxygenation of triglycerides in N_2 atmosphere [18–20]. Solid acid catalysts possess relatively high activities; however, hydrocarbons with long carbon chains (heavy hydrocarbons) crack on the acid sites [18]. This is unfortunate, because, in general, heavy hydrocarbons have a high value as chemicals and transport fuels. In contrast, the activities of solid base catalysts are relatively low; moreover, they exhibit relatively high selectivity for heavy hydrocarbons [19,20]. Pd supported on active carbon (Pd/C) has been reported as an effective catalyst for the catalytic deoxygenation of fatty acids and their esters in He atmosphere [14,21].

In this study, we chose hexadecyl palmitate ($C_{15}H_{31}COOC_{16}H_{33}$) as a model compound of Euglena oil. We developed a highly active Pd/Mg(Al)O catalyst (derived from Pd-containing MgAl-type hydrotalcite) for the deoxygenation of $C_{15}H_{31}COOC_{16}H_{33}$ to hydrocarbons in H_2 and N_2 atmospheres.

2. Results and Discussion

2.1. Catalyst Characterization

Figure 1 shows a structural model of the $Pd_{0.016}Mg_3Al(OH)_{16}CO_3{\cdot}xH_2O$ hydrotalcite used in this study. Hydrotalcite is a kind of anion clay with the general formula $[M^{2+}{}_{1-m}M^{3+}{}_m(OH)_2]^{m+}A^{n-}{}_{m/n}{\cdot}xH_2O$ (M^{2+}, M^{3+} = metal cations, A^{n-} = interlayer anion) [22]. The metal cations are distributed in brucite-like layers, and the interlayer anions are fixed between the brucite-like layers by electric charge interaction. The M^{2+} cation is usually Mg^{2+} and the M^{3+} cation is usually Al^{3+}. The noble metal Pd^{2+} cation can be introduced into the M^{2+} position when $Pd^{2+}/(M^{2+} + M^{3+}) <$ 5 mo % [23–25]. Basic MgAl-type hydrotalcite is the most common hydrotalcite, and has been used as an effective catalyst for some industrially important reactions [22–29].

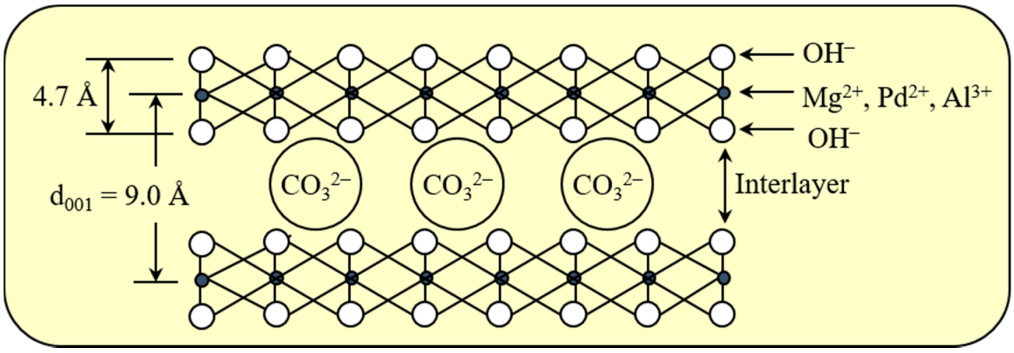

Figure 1. Structural model of the $Pd_{0.016}Mg_3Al(OH)_{16}CO_3{\cdot}xH_2O$ hydrotalcite used in this study.

Figure 2 shows X-ray diffraction (XRD) patterns of $Pd_{0.016}Mg_3Al(OH)_{16}CO_3{\cdot}xH_2O$ after drying at 100 °C. By using a JICST database (from The Crystallographic Society of Japan) for identification, only the well-crystallized $Mg_3Al(OH)_{16}CO_3$ phase was observed in the XRD pattern of $Pd_{0.016}Mg_3Al(OH)_{16}CO_3{\cdot}xH_2O$. The peaks of $Pd(OH)_2$ and PdO phases could not be observed in the XRD pattern, probably because they formed amorphous phases. It is also possible that the Pd^{2+} ions entered the Mg^{2+} position in $Pd_{0.016}Mg_3Al(OH)_{16}CO_3{\cdot}xH_2O$ at a low Pd content [25]. The *d* (001) (basal *d*) spacing at the lowest angle in the XRD pattern was 9.0 Å for $Pd_{0.016}Mg_3Al(OH)_{16}CO_3{\cdot}xH_2O$. As shown in Figure 1, the thickness of the MgAl-type brucite-like layer was 4.7 Å [22]. The gallery height was 4.3 Å in $Pd_{0.016}Mg_3Al(OH)_{16}CO_3{\cdot}xH_2O$ after subtracting the thickness of the MgAl-type hydrotalcite layer (4.7 Å) from the basal *d* spacing (9.0 Å). This gallery height (4.3 Å) coincides with the size of the CO_3^{2-} anion [22].

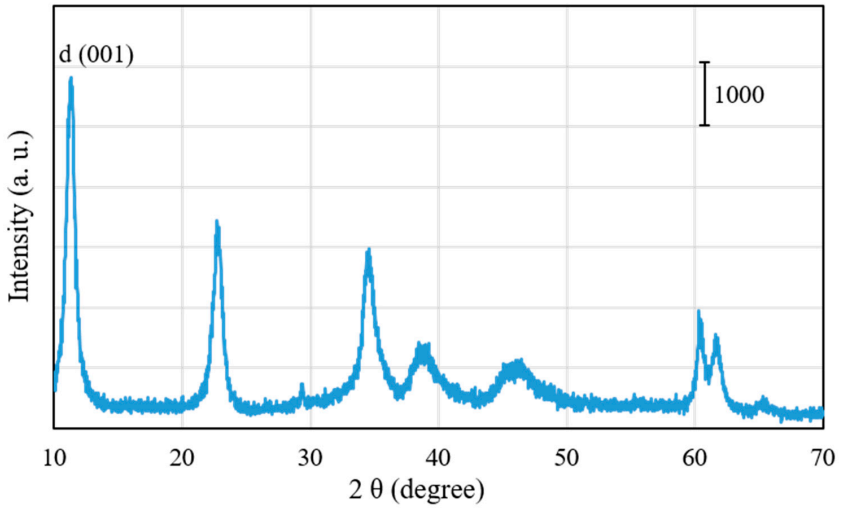

Figure 2. X-ray diffraction (XRD) patterns of $Pd_{0.016}Mg_3Al(OH)_{16}CO_3 \cdot xH_2O$ after drying at 100 °C.

Figure 3 shows the thermogravimetric analysis (TGA) and differential thermal analysis (DTA) results for $Pd_{0.016}Mg_3Al(OH)_{16}CO_3 \cdot xH_2O$ after drying at 100 °C. Three stages of sudden weight loss can be observed in the TGA curve. The first sudden weight loss, which appears at below 200 °C, was attributed to the loss of physically absorbed water and interlayer water. The second sudden weight loss, at 220–450 °C, was attributed to the removal of CO_2 from the interlayer carbonate anions and hydroxyl groups from the brucite-like layers. The third sudden weight loss, at 850–890 °C, can be ascribed to the formation of the spinel-like phase of $MgAl_2O_4$ [20,24]. The results of DTA and TGA nearly coincide. The endotherm band at 130 °C in the DTA curve corresponds to the loss of physically absorbed water. After losing physically absorbed water, $Pd_{0.016}Mg_3Al(OH)_{16}CO_3 \cdot xH_2O$ was converted to $Pd_{0.016}Mg_3Al(OH)_{16}CO_3 \cdot 4H_2O$. The endotherm band at 190 °C in the DTA curve corresponds to the loss of interlayer water. After losing interlayer water, $Pd_{0.016}Mg_3Al(OH)_{16}CO_3 \cdot 4H_2O$ was converted to $Pd_{0.016}Mg_3Al(OH)_{16}CO_3$. The endotherm band at 420 °C in the DTA curve corresponds to the loss of interlayer carbonate anions and hydroxyl groups in the brucite-like layers. The layered structure of hydrotalcite was destroyed upon calcination at 420 °C, following which $Pd_{0.016}Mg_3Al(OH)_{16}CO_3$ was converted to a metal–oxide mixture $Pd_{0.016}Mg_3AlO_x$, in which Pd^{2+} and Al^{3+} ions entered the MgO cubic lattices [22]. The small endotherm band at 860 °C in the DTA curve corresponds to the solid phase change of the metal–oxide mixture to a spinel-like phase of $MgAl_2O_4$ and crystalline MgO [22].

Figure 4 shows the dependence of the Brunauer-Emmett-Teller (BET) surface area of $Pd_{0.016}Mg_3Al(OH)_{16}CO_3 \cdot xH_2O$ on calcination temperature from 100 °C to 1000 °C. Calcination was carried out at each temperature for 3 h in air. $Pd_{0.016}Mg_3Al(OH)_{16}CO_3 \cdot xH_2O$ showed a BET surface area of 73 m^2/g after calcination at 100 °C. The BET surface area increased with an increasing calcination temperature from 100 °C to 450 °C, and then decreased with increasing calcination temperature from 450 °C to 1000 °C. The layered structure of $Pd_{0.016}Mg_3Al(OH)_{16}CO_3$ hydrotalcite was destroyed, and a PdO-Mg(Al)O metal-oxide mixture was formed upon calcination at 450 °C. In the process of destruction, the removal of CO_2 (from the interlayer carbonate anions) and hydroxyl groups (from the brucite-like layers) created pores in the PdO-Mg(Al)O metal-oxide mixture formed. These pores increased the BET surface area. Calcination at a temperature that was higher than 450 °C caused sintering of the metal-oxide mixture particles, which decreased the BET surface area. Moreover, an obvious decrease in the BET surface area was observed at 800–850 °C. The formation of spinel-like phases of $MgAl_2O_4$ from the PdO-Mg(Al)O metal-oxide mixture resulted in a decrease in the BET surface area upon calcination at 800–850 °C [25]. Because the highest BET surface area (143 m^2/g) was obtained for calcination at 450 °C, we calcined $Pd_{0.016}Mg_3Al(OH)_{16}CO_3 \cdot xH_2O$ at 450 °C for 3 h in air before use in this study.

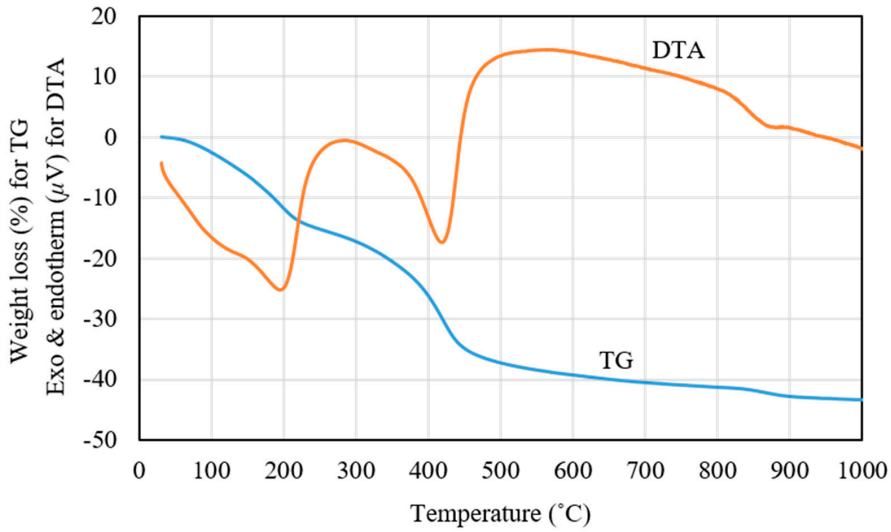

Figure 3. The thermogravimetric analysis (TGA) and differential thermal analysis (DTA) results for $Pd_{0.016}Mg_3Al(OH)_{16}CO_3 \cdot xH_2O$ after drying at 100 °C.

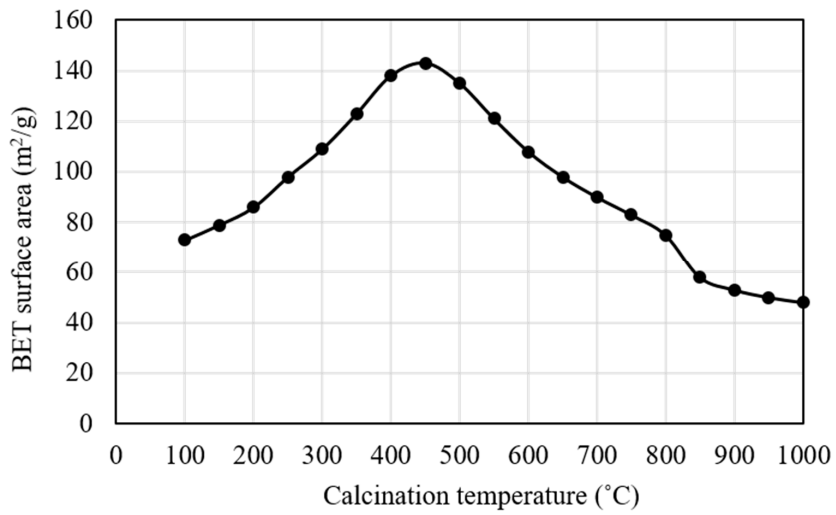

Figure 4. The Brunauer-Emmett-Teller (BET) surface area of $Pd_{0.016}Mg_3Al(OH)_{16}CO_3 \cdot xH_2O$ on calcination temperature from 100 °C to 1000 °C.

The use of uniform multicomponent precursors results in well-dispersed metal particles on the surface of supports after calcination and reduction. This method, known as "solid phase crystallization" (SPC), is important in the preparation of highly active metal-supported catalysts [27–35]. In this study, Pd^{2+} could enter the Mg^{2+} position in $Pd_{0.016}Mg_3Al(OH)_{16}CO_3 \cdot xH_2O$ hydrotalcite after drying at 100 °C in air. As a result, a well-distributed mixed oxide, PdO-Mg(Al)O, could be formed after calcining $Pd_{0.016}Mg_3Al(OH)_{16}CO_3 \cdot xH_2O$ at 450 °C in air. Finally, a Pd/Mg(Al)O catalyst with highly dispersed Pd metal particles and strong interaction between the metal and support could be obtained after the pretreatment process of H_2 flow reduction.

2.2. Catalytic Deoxygenation of $C_{15}H_{31}COOC_{16}H_{33}$ in H_2 Atmosphere

Figure 5 shows the flame ionization detector–gas chromatography (FID-GC) charts of $C_{15}H_{31}COOC_{16}H_{33}$ and the liquid product formed upon deoxygenation of $C_{15}H_{31}COOC_{16}H_{33}$ in H_2 atmosphere, at 300 °C, for 2 h, over 1 wt.% Pd/Mg(Al)O catalyst. As shown in Figure 5B, the reactant ($C_{15}H_{31}COOC_{16}H_{33}$) peak is not observed in the GC chart after reaction at 300 °C for 2 h. The liquid

products were almost saturated hydrocarbons n-$C_{16}H_{34}$ and n-$C_{15}H_{32}$. By calculating the amount of each component in the product using the GC chart, the molar ratio of n-$C_{16}H_{34}$ to n-$C_{15}H_{32}$ in the liquid product was found to be 4.3.

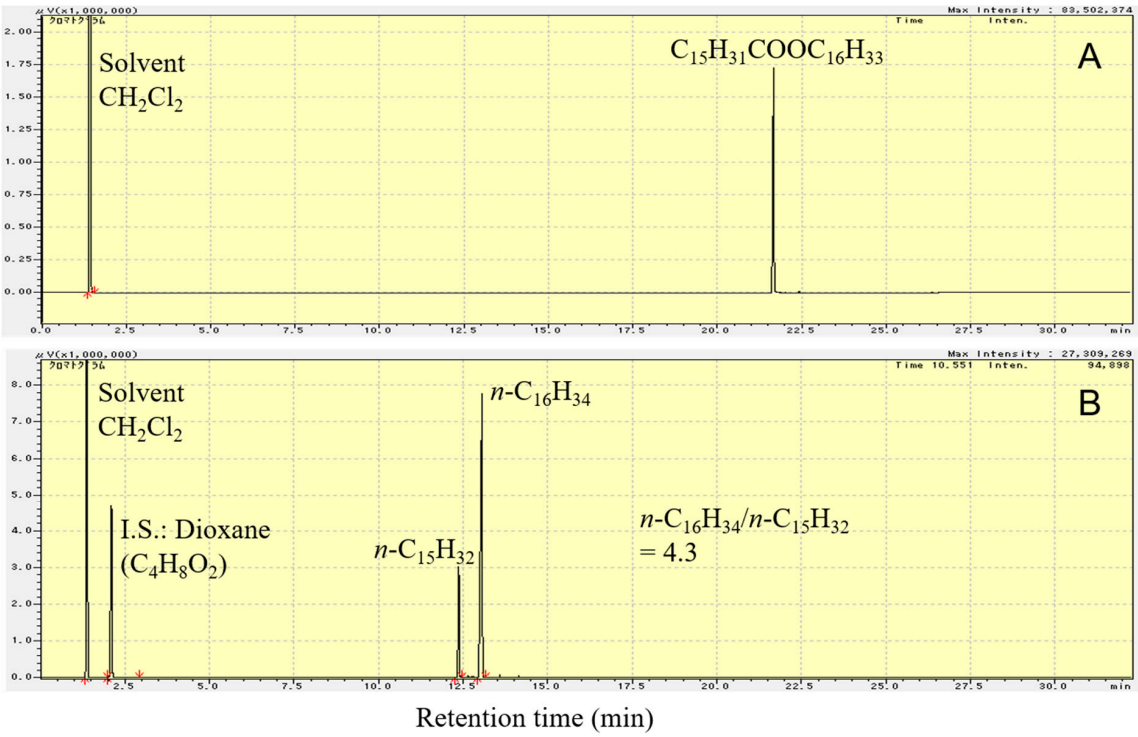

Figure 5. The flame ionization detector–gas chromatography (FID-GC) charts of $C_{15}H_{31}COOC_{16}H_{33}$ (**A**) and the liquid product formed upon deoxygenation of $C_{15}H_{31}COOC_{16}H_{33}$ in H_2 atmosphere, at 300 °C, for 2 h, over 1 wt.% Pd/Mg(Al)O catalyst (**B**). Reaction conditions: $C_{15}H_{31}COOC_{16}H_{33}$: 5 g; catalyst: 0.2 g; and, H_2 pressure at 25 °C: 0.9 MPa.

As shown in Reactions (1)–(3), deoxygenation of saturated fatty acids (such as stearic acid $C_{17}H_{35}COOH$) involves three parallel reactions: reduction, decarbonylation, and decarboxylation [7]. For a fatty acid having an even number of carbons, reduction produces a normal paraffin having an even number of carbons plus water; decarbonylation produces a normal paraffin having an odd number of carbons plus water and CO; and, decarboxylation produces a normal paraffin having an odd number of carbons plus CO_2.

$$C_{17}H_{35}COOH + 3H_2 = C_{18}H_{38} + 2H_2O \text{ Reduction} \quad (1)$$

$$C_{17}H_{35}COOH + H_2 = C_{17}H_{36} + CO + H_2O \text{ Decarbonylation} \quad (2)$$

$$C_{17}H_{35}COOH = C_{17}H_{36} + CO_2 \text{ Decarboxylation} \quad (3)$$

Based on Reactions (1)–(3), we believe that the deoxygenation of $C_{15}H_{31}COOC_{16}H_{33}$ in H_2 atmosphere over 1 wt.% Pd/Mg(Al)O also involves three parallel reactions: reduction (Reaction (4)), decarbonylation (Reaction (5)), and decarboxylation (Reaction (6)).

$$C_{15}H_{31}COOC_{16}H_{33} + 4H_2 = 2C_{16}H_{34} + 2H_2O \text{ Reduction} \quad (4)$$

$$C_{15}H_{31}COOC_{16}H_{33} + 2H_2 = C_{15}H_{32} + C_{16}H_{34} + CO + H_2O \text{ Decarbonylation} \quad (5)$$

$$C_{15}H_{31}COOC_{16}H_{33} + H_2 = C_{15}H_{32} + C_{16}H_{34} + CO_2 \text{ Decarboxylation} \quad (6)$$

As shown in Reactions (4)–(6), the reduction of one $C_{15}H_{31}COOC_{16}H_{33}$ molecule produces two $C_{16}H_{34}$ molecules. On the other hand, either decarbonylation or decarboxylation of one $C_{15}H_{31}COOC_{16}H_{33}$ molecule produces one $C_{16}H_{34}$ molecule and one $C_{15}H_{32}$ molecule. The decarbonylation of $C_{15}H_{31}COOC_{16}H_{33}$ produces CO, whereas the decarboxylation of $C_{15}H_{31}COOC_{16}H_{33}$ produces CO_2. Both CO and CO_2 were detected in the gas product from the reaction over 1 wt.% Pd/Mg(Al)O catalyst, indicating that both decarbonylation of $C_{15}H_{31}COOC_{16}H_{33}$ (Reaction (5)) and decarboxylation of $C_{15}H_{31}COOC_{16}H_{33}$ (Reaction (6)) occurred during the reaction. Moreover, among Reactions (4)–(6), the reduction of $C_{15}H_{31}COOC_{16}H_{33}$ (Reaction (4)) was the main reaction, because the quantity of *n*-$C_{16}H_{34}$ in the liquid product was much more than that of *n*-$C_{15}H_{32}$ (Figure 5B).

For deoxygenation of $C_{15}H_{31}COOC_{16}H_{33}$ in H_2 atmosphere, the metal site alone could achieve a high activity, because deoxygenation was carried out via three routes: reduction, decarbonylation, and decarboxylation. We used an acid support for the metal in order to adjust the selectivity of the hydrocarbon products during deoxygenation in H_2 atmosphere [6,7]. In this study, we used a base support (Mg(Al)O) for the metal (Pd) in order to suppress the hydrocracking of *n*-$C_{15}H_{32}$ and *n*-$C_{16}H_{34}$ products (to light hydrocarbons) during deoxygenation of $C_{15}H_{31}COOC_{16}H_{33}$ in H_2 atmosphere.

Figure 6 shows X-ray diffraction (XRD) patterns of 1 wt.% Pd/Mg(Al)O catalyst before reaction and after reaction (for deoxygenation of $C_{15}H_{31}COOC_{16}H_{33}$ in H_2 atmosphere at 300 °C for 2 h). The sample before reaction was obtained by calcining $Pd_{0.016}Mg_3Al(OH)_{16}CO_3 \cdot xH_2O$ in air at 450 °C for 3 h, and then reducing in H_2 at 300 °C for 1 h. The XRD pattern of the sample before reaction proved the formation of mixed Mg-Al oxides phases, indicating that the decomposition of the layered structure occurred after calcination and reduction. The reflections in XRD pattern at about 43° and 63° corresponded to MgO-like phase (periclase), or rather MgO-Al_2O_3 solid solution Mg(Al)O [22]. The reflection of Al_2O_3 phase at 23° was very small, indicating that Al^{3+} cations were dispersed in the structure of MgO without the formation of spinel species. Because the Pd loading was low (1 wt.%) in the Pd/Mg(Al)O catalyst, the metal Pd crystals certainly formed in very small sizes, and thus the metal Pd phase could not be detected in the XRD pattern. The sample after reaction was obtained by filtrating out liquid products, and then drying in vacuum at room temperature for 10 h. From a comparison of the XRD pattern of Pd/Mg(Al)O catalyst before reaction, no obvious change could be observed in the XRD patterns of Pd/Mg(Al)O catalyst after reaction in H_2 atmosphere at 300 °C for 2 h.

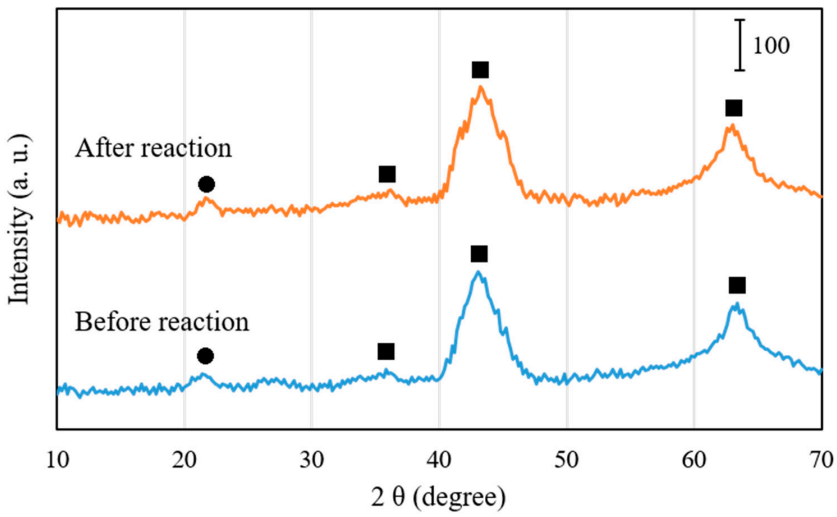

Figure 6. X-ray diffraction (XRD) patterns of 1 wt.% Pd/Mg(Al)O catalyst before reaction and after reaction (for deoxygenation of $C_{15}H_{31}COOC_{16}H_{33}$ in H_2 atmosphere at 300 °C for 2 h). ■, MgO; ●, Al_2O_3.

Figure 7 shows the dependence of $C_{15}H_{31}COOC_{16}H_{33}$ conversion and C_{10}–C_{16} hydrocarbon yield on the reaction time for the catalytic deoxygenation of $C_{15}H_{31}COOC_{16}H_{33}$ in H_2 atmosphere, at 300 °C, over 1 wt.% Pd/Mg(Al)O catalyst. Four autoclave reactors were charged with the same reactant gases and the same amount of catalyst, and then operated at the same temperature (300 °C). The reaction in each autoclave reactor was finished in an hour. The products were analysed to determine the $C_{15}H_{31}COOC_{16}H_{33}$ conversion and the C_{10}–C_{16} hydrocarbon yield at that reaction time. The yield of C_{10}–C_{16} hydrocarbons is important as they can be used as aviation fuel [16]. As shown in Figure 7, $C_{15}H_{31}COOC_{16}H_{33}$ conversion increased with the reaction time, and approached 100% after reaction for 2 h in H_2 atmosphere. CO and CO_2, which formed from decarbonylation and decarboxylation of $C_{15}H_{31}COOC_{16}H_{33}$ (Reactions (5) and (6)) were the main by-products in the deoxygenation of $C_{15}H_{31}COOC_{16}H_{33}$ in H_2 atmosphere [6,7]. The amounts of formed CO and CO_2 almost kept constant after reaction for 2 h. A small amount of C_1–C_4 gaseous hydrocarbons was also formed during the reaction in H_2 atmosphere, and the amount of C_1–C_4 gaseous hydrocarbons increased with prolonging the reaction time. As shown in Figure 7, the yield of C_1-C_{16} hydrocarbons increased to 90.2% after reaction for 2 h, and then decreased slightly with prolonging reaction time due to the formation of light hydrocarbons (<C_9). On the whole, the Pd/Mg(Al)O catalyst provided a high catalytic performance for the catalytic deoxygenation of $C_{15}H_{31}COOC_{16}H_{33}$ to hydrocarbons in H_2 atmosphere.

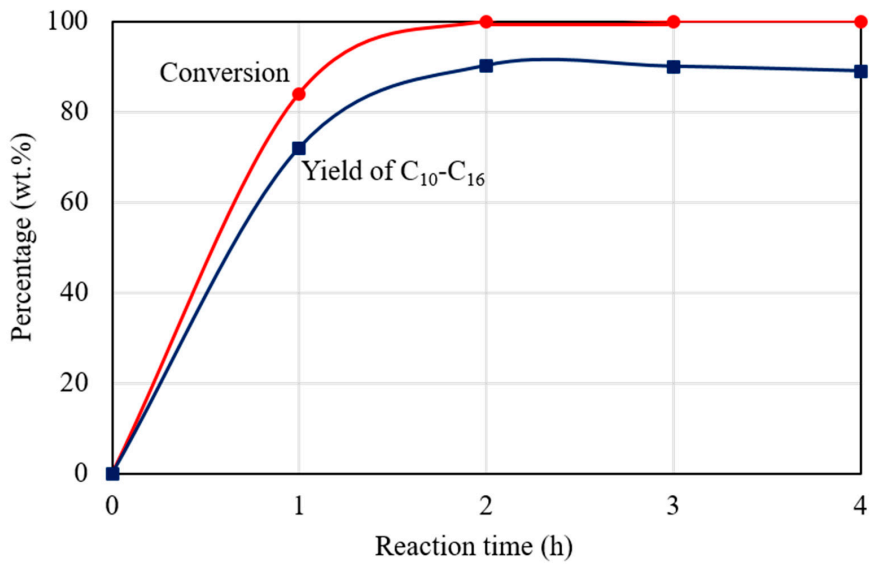

Figure 7. The dependence of $C_{15}H_{31}COOC_{16}H_{33}$ conversion and C_{10}–C_{16} hydrocarbon yield on the reaction time for the catalytic deoxygenation of $C_{15}H_{31}COOC_{16}H_{33}$ in H_2 atmosphere, at 300 °C, over 1 wt.% Pd/Mg(Al)O catalyst. Reaction conditions: $C_{15}H_{31}COOC_{16}H_{33}$: 5 g; catalyst: 0.2 g; H_2 pressure at 25 °C: 0.9 MPa.

2.3. Catalytic Deoxygenation of $C_{15}H_{31}COOC_{16}H_{33}$ in N_2 Atmosphere

Table 1 shows the $C_{15}H_{31}COOC_{16}H_{33}$ conversion and C_{10}–C_{16} hydrocarbons yield of the deoxygenation of $C_{15}H_{31}COOC_{16}H_{33}$ in N_2 atmosphere at 300 °C for 2 h over various catalysts. The 1 wt.% Pd/Mg(Al)O catalyst resulted in a $C_{15}H_{31}COOC_{16}H_{33}$ conversion of 76.4% and a C_{10}–C_{16} yield of 63.5% for the reaction at 300 °C for 2 h in N_2 atmosphere. Both, $C_{15}H_{31}COOC_{16}H_{33}$ conversion and the C_{10}–C_{16} yield obtained in N_2 atmosphere, were much lower than those obtained in H_2 atmosphere (Figure 6) over Pd/Mg(Al)O after reaction at 300 °C for 2 h. This indicates that H_2 greatly improves the deoxygenation of $C_{15}H_{31}COOC_{16}H_{33}$, and that it is difficult to produce hydrocarbons from $C_{15}H_{31}COOC_{16}H_{33}$ in N_2 atmosphere. The use of basic hydrotalcite, acidic H-ZSM-5, and Pd/C has been reported for the deoxygenation of triglycerides or fatty acids in N_2 or Ar atmospheres [14,17,18]. As shown in Table 1, the basic catalyst Mg(Al)O without Pd gave low conversion (23.3%) and a low

yield of C_{10}–C_{16} hydrocarbons (15.1%) for the reaction in N_2 atmosphere. In contrast, the conversion was relatively high (55.6%), but the yield of C_{10}–C_{16} hydrocarbons was very low (8.3%) over the acidic catalyst H-ZSM-5. Heavy hydrocarbons formed in the reaction cracked to light hydrocarbons on the acidic sites of H-ZSM-5 during the reaction. The use of Pd/C resulted in a $C_{15}H_{31}COOC_{16}H_{33}$ conversion of 41.7% and a C_{10}–C_{16} hydrocarbons yield of 26.2% for the reaction at 300 °C for 2 h in N_2 atmosphere. Therefore, Pd/Mg(Al)O shows a much higher catalytic performance than these catalysts that are reported in the literature, for the deoxygenation of $C_{15}H_{31}COOC_{16}H_{33}$ in N_2 atmosphere. The development of multi-functional catalysts to improve catalyst performance is an important challenge in the catalyst field. The catalyst containing Pt metal and basic hydrotalcite has been reported as excellent for the aromatization of n-hexane [26]. We had developed some multi-functional catalysts containing metal and solid acid for some industrially important reactions [36–42]. Pd metal sites and solid base sites (in Mg(Al)O) achieved a synergetic effect for the deoxygenation of $C_{15}H_{31}COOC_{16}H_{33}$ in N_2 atmosphere over the Pd/Mg(Al)O catalyst.

Table 1. The $C_{15}H_{31}COOC_{16}H_{33}$ conversion and C_{10}–C_{16} hydrocarbons yield of the deoxygenation of $C_{15}H_{31}COOC_{16}H_{33}$ in N_2 atmosphere at 300 °C for 2 h over various catalysts [a].

Catalyst	Conversion (%)	Yield (%)			
		C_1–C_4	C_5–C_9	C_{10}–C_{16}	CO_2
Pd/Mg(Al)O [b]	76.4	1.4	3.6	63.5	4.8
Mg(Al)O	23.3	0.5	1.7	15.1	1.6
H-ZSM-5	55.6	5.8	26.3	8.3	3.1
Pd/C [b]	41.7	1.2	4.1	26.2	2.7

[a] Reaction conditions: $C_{15}H_{31}COOC_{16}H_{33}$: 5 g; catalyst: 0.2 g; N_2 pressure at 25 °C: 0.9 MPa. [b] Pd loading: 1 wt.%.

Figure 8 shows the FID-GC charts of the liquid product formed by deoxygenation of $C_{15}H_{31}COOC_{16}H_{33}$ in N_2 atmosphere at 300 °C for 2 h over 1 wt.% Pd/Mg(Al)O catalyst. A comparison of Figures 5B and 8A shows that the peak of the $C_{15}H_{31}COOC_{16}H_{33}$ reactant still appears in the GC chart after reaction in N_2 atmosphere. For the deoxygenation of $C_{15}H_{31}COOC_{16}H_{33}$ over the Pd/Mg(Al)O catalyst, the reaction rate in N_2 atmosphere was slow in comparison with that in the H_2 atmosphere. The reaction in N_2 atmosphere formed some compounds with a retention time ranging from 14 to 22 min in the GC chart (fatty acid, alcohol, and ketones). These compounds decreased the yield of hydrocarbons from the deoxygenation of $C_{15}H_{31}COOC_{16}H_{33}$. Moreover, peaks of C_5–C_{14} hydrocarbons appear in the GC chart of the 2 h reaction in N_2 atmosphere (Figure 8A). Figure 8B shows the magnified area from 11.1 to 14.1 min in Figure 8A; this enables us to observe the composition of C_{15} and C_{16} hydrocarbons that are formed by the reaction in N_2 atmosphere. As shown in Figure 5B, deoxygenation of $C_{15}H_{31}COOC_{16}H_{33}$ in H_2 atmosphere only formed normal paraffin hydrocarbons. As shown in Figure 8B, the hydrocarbon products that are formed by the deoxygenation of $C_{15}H_{31}COOC_{16}H_{33}$ in N_2 atmosphere contained *n*-paraffin and several kinds of olefins. A comparison of the GC-MS results with values in the NIST-11 database indicates that the peaks around n-paraffin were olefins with the same number of carbon chains. The initially formed olefins were converted into other olefins by double bond migration on the basic sites of Mg(Al)O. Solid base catalysts (such as MgO) have the catalytic ability for double bond migration of olefins [43]. By calculating the amount of each component in the product using the GC chart, the amount of total C_{16} hydrocarbons and the amount of total C_{15} hydrocarbons was found to be almost the same in the liquid product that was formed from the catalytic deoxygenation of $C_{15}H_{31}COOC_{16}H_{33}$ in N_2 atmosphere, at 300 °C, for 2 h, over the Pd/Mg(Al)O catalyst.

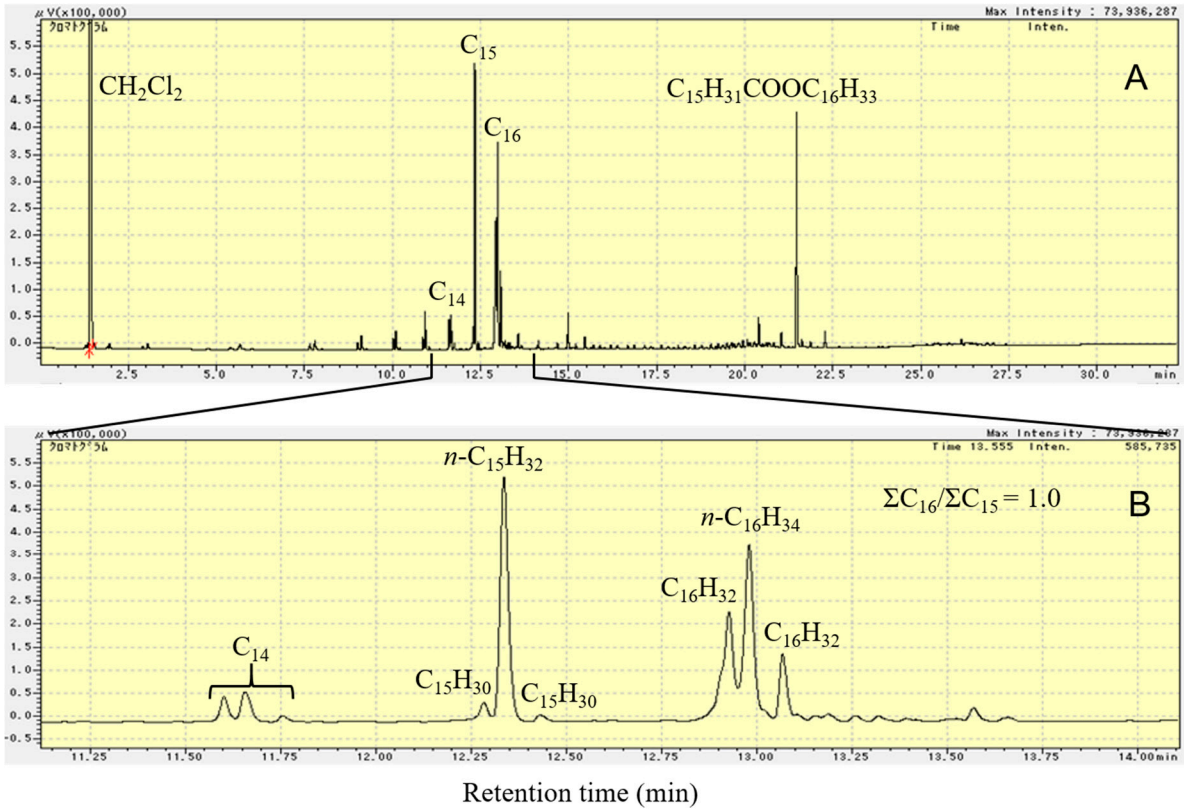

Figure 8. The FID-GC charts of the liquid product formed by deoxygenation of $C_{15}H_{31}COOC_{16}H_{33}$ in N_2 atmosphere at 300 °C for 2 h over 1 wt.% Pd/Mg(Al)O catalyst. (**A**): retention time from 0 to 32 min, (**B**): retention time from 11.1 to 14.1 min. Reaction conditions: $C_{15}H_{31}COOC_{16}H_{33}$: 5 g; catalyst: 0.2 g; N_2 pressure at 25 °C: 0.9 MPa.

Reactions (7) and (8) show the reactions for the deoxygenation of $C_{15}H_{31}COOC_{16}H_{33}$ in N_2 (without H_2) atmosphere. CO could not be detected in the gas products of the reaction in N_2 atmosphere, thus, decarboxylation was deduced to be the only reaction in the deoxygenation of $C_{15}H_{31}COOC_{16}H_{33}$ in N_2 atmosphere.

$$C_{15}H_{31}COOC_{16}H_{33} = C_{15}H_{32} + C_{16}H_{32} + CO_2 \text{ Decarboxylation} \quad (7)$$

$$C_{15}H_{31}COOC_{16}H_{33} = C_{15}H_{30} + C_{16}H_{34} + CO_2 \text{ Decarboxylation} \quad (8)$$

In N_2 atmosphere, the number of H atoms in the $C_{15}H_{31}COOC_{16}H_{33}$ molecule was not enough to obtain the saturated hydrocarbons $C_{16}H_{34}$ and $C_{15}H_{32}$ in the decarboxylation of $C_{15}H_{31}COOC_{16}H_{33}$. One $C_{15}H_{31}COOC_{16}H_{33}$ molecule must form one paraffin and one olefin by decarboxylation without H_2. The high reactivity of the olefin molecules formed resulted in the formation of light hydrocarbons. A few heavy hydrocarbons larger than C_{16} were also formed by the polymerization of light olefins. Because both Reactions (7) and (8) form the same amount of C_{15} and C_{16} hydrocarbons, the molar ratio of total C_{16} hydrocarbons to total C_{15} hydrocarbons was 1.0, as shown in Figure 8B. Moreover, the ratio of n-$C_{15}H_{32}$ in the total C_{15} hydrocarbons was much higher than the ratio of n-$C_{16}H_{34}$ in the total C_{16} hydrocarbons (Figure 8B). Thus, Reaction (7) was the main decarboxylation reaction (as compared to Reaction (8)) in the catalytic deoxygenation of $C_{15}H_{31}COOC_{16}H_{33}$ in N_2 atmosphere.

For deoxygenation of $C_{15}H_{31}COOC_{16}H_{33}$ in N_2 atmosphere, the metal site alone could not achieve enough activity, because deoxygenation was carried out via a single route, namely decarboxylation. In this study, we used a base support (Mg(Al)O) for the metal (Pd) in order to enhance the catalytic activity during deoxygenation of $C_{15}H_{31}COOC_{16}H_{33}$ in N_2 atmosphere.

Figure 9 shows the dependence of $C_{15}H_{31}COOC_{16}H_{33}$ conversion and C_{10}–C_{16} hydrocarbons yield on reaction time for the catalytic deoxygenation of $C_{15}H_{31}COOC_{16}H_{33}$ in N_2 atmosphere, at 300 °C, over the 1 wt.% Pd/Mg(Al)O catalyst. $C_{15}H_{31}COOC_{16}H_{33}$ conversion increased with prolonged reaction time and reached 100% after reaction for 6 h. The yield of C_{10}–C_{16} hydrocarbons increased with prolonged reaction until 5 h, and then decreased slightly due to the formation of light hydrocarbons. Although the catalytic activity in N_2 atmosphere was lower than that in the H_2 atmosphere, the Pd/Mg(Al)O catalyst yielded a $C_{15}H_{31}COOC_{16}H_{33}$ conversion of 99.1% and a C_{10}–C_{16} hydrocarbon yield of 80.4% by prolonging reaction time to 5 h for the reaction in N_2 atmosphere at 300 °C.

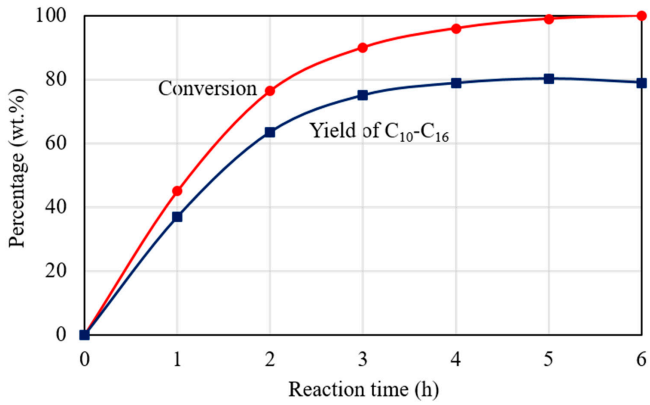

Figure 9. The dependence of $C_{15}H_{31}COOC_{16}H_{33}$ conversion and C_{10}–C_{16} hydrocarbons yield on reaction time for the catalytic deoxygenation of $C_{15}H_{31}COOC_{16}H_{33}$ in N_2 atmosphere, at 300 °C, over the 1 wt.% Pd/Mg(Al)O catalyst. Reaction conditions: $C_{15}H_{31}COOC_{16}H_{33}$: 5 g; catalyst: 0.2 g; N_2 pressure at 25 °C: 0.9 MPa.

Figure 10 shows the dependence of $C_{15}H_{31}COOC_{16}H_{33}$ conversion and C_{10}–C_{16} hydrocarbon yield on reaction temperature for the catalytic deoxygenation of $C_{15}H_{31}COOC_{16}H_{33}$ in N_2 atmosphere, for 2 h, over the 1 wt.% Pd/Mg(Al)O catalyst. $C_{15}H_{31}COOC_{16}H_{33}$ conversion increased with an increasing reaction temperature from 275 to 375 °C, and achieved a conversion of over 99% for the reaction at 375 °C for 2 h. The yield of C_{10}–C_{16} hydrocarbons increased with an increasing reaction temperature from 275 to 325 °C. At a reaction temperature higher than 325 °C, the yield of C_{10}–C_{16} hydrocarbons could not be improved by increasing the reaction temperature because the number of light hydrocarbons ($<C_9$) in the product increased at high reaction temperatures.

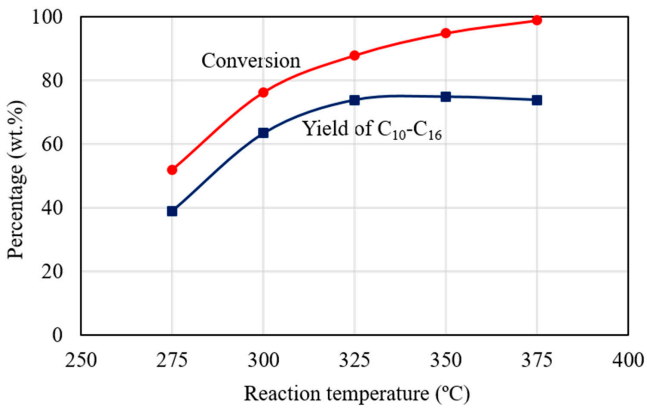

Figure 10. The dependence of $C_{15}H_{31}COOC_{16}H_{33}$ conversion and C_{10}–C_{16} hydrocarbon yield on reaction temperature for the catalytic deoxygenation of $C_{15}H_{31}COOC_{16}H_{33}$ in N_2 atmosphere, for 2 h, over the 1 wt.% Pd/Mg(Al)O catalyst. Reaction conditions: $C_{15}H_{31}COOC_{16}H_{33}$: 5 g; catalyst: 0.2 g; N_2 pressure at 25 °C: 0.9 MPa.

3. Experimental Section

3.1. Reagents

Hexadecyl palmitate ($C_{15}H_{31}COOC_{16}H_{33}$) of purity higher than 95% was purchased from Tokyo Chemical Industry Co., Ltd. (Tokyo, Japan) Na-ZSM-5 zeolite (SiO_2/Al_2O_3 = 50) was purchased from Wako Pure Chemical Industries, Ltd. (Tokyo, Japan) Activated carbon (C), with a particle size of 100 mesh, was purchased from Aldrich Chem. Co. Inc. (Milwaukee, WI, USA); the BET surface area of the C support was 593 m^2/g by N_2 adsorption measurement. Other chemical reagents were purchased from Wako Pure Chemical Industries Ltd. (Tokyo, Japan) with purities higher than 99%. Gas cylinders were purchased from Sumitomo Seika Chemicals Co., Ltd. (Tokyo, Japan) with purities higher than 99.995%.

3.2. Catalysts

$Pd_{0.016}Mg_3Al(OH)_{16}CO_3{\cdot}xH_2O$ hydrotalcite was prepared using a co-precipitation method at pH 10.0, by adding an aqueous solution containing $Pd(NO_3)_2$, $Mg(NO_3)_2$, and $Al(NO_3)_3$ (the molar ratio of Pd to Mg to Al was 0.016:3:1) to a solution containing a slight excess of Na_2CO_3 at 65 °C. A 1 M NaOH aqueous solution was added during the process to maintain the pH value at 10.0. After standing at 65 °C for 4 h, a precipitate was obtained by filtration. The resultant precipitate was dried in air at 100 °C for 24 h.

The Pd/Mg(Al)O catalyst was obtained by reducing PdO-Mg(Al)O mixed oxide under H_2 flow (60 mL/min) at 300 °C for 1 h. The PdO-Mg(Al)O mixed oxide was obtained by calcining $Pd_{0.016}Mg_3Al(OH)_{16}CO_3{\cdot}xH_2O$ hydrotalcite in air at 450 °C for 3 h. By calculating the amount of Pd in the $Pd_{0.016}Mg_3Al(OH)_{16}CO_3{\cdot}4H_2O$ precursor, the designed Pd loading was determined to be about 1 wt.% in the Pd/Mg(Al)O catalyst. The actual amount of Pd loading (measured by elemental analysis) was 0.95 wt.% in the Pd/Mg(Al)O catalyst.

Mg(Al)O was obtained by calcination of $Mg_3Al(OH)_{16}CO_3{\cdot}xH_2O$ hydrotalcite in air at 450 °C for 3 h. $Mg_3Al(OH)_{16}CO_3{\cdot}xH_2O$ hydrotalcite was prepared by a co-precipitation method at pH 10.0, by adding an aqueous solution containing $Mg(NO_3)_2$ and $Al(NO_3)_3$ (molar ratio of Mg to Al was 3) to a solution containing a slight excess of Na_2CO_3 at 65 °C. A 1 M NaOH aqueous solution was added during the process to maintain the pH value at 10.0. The resultant precipitate was washed and dried in air at 100 °C for 24 h.

H-ZSM-5 was prepared using Na-ZSM-5 as follows. Na-ZSM-5 was treated with an aqueous solution of NH_4NO_3 (0.1 M) to form NH_4-ZSM-5 by ion exchange. After filtering out the water, the NH_4-ZSM-5 obtained was dried in air at 100 °C for 24 h, and then calcined in air at 550 °C for 3 h to form H-ZSM-5.

Pd/C was synthesized by using a wet impregnation method. The activated carbon support was impregnated with an aqueous solution of $Pd(NO_3)_2$ with stirring. After removal of the solvent by heating at 90 °C, the resultant solid product was dried in air at 100 °C for 24 h. Then, Pd/C was calcined under a N_2 flow (60 mL/min) at 400 °C for 1 h to remove NO_3^- ions. In the Pd/C catalyst, the designed Pd loading was 1 wt.% and the actual amount of Pd loading (measured by element analysis) was 1.02 wt.%.

3.3. Instruments

Powder X-ray diffraction (XRD) patterns were measured using a MAC Science MXP-18 diffractometer (XrayScience Corp., Tokyo, Japan) with Cu Kα radiation operated at 40 kV and 50 mA. The solid phase was identified by referring to the JICST database (Version 6th, Japan Information Center of Science and Technology, Tokyo, Japan, 2012) from The Crystallographic Society of Japan. Thermogravimetric and differential thermal analyses (TG-DTA) were carried out using a Shimadzu TGA-50 instrument (Shimadzu Corp., Kyoto, Japan). The sample was heated under an atmosphere of N_2 flow (60 mL/min) at a heating rate of 5 °C/min from room temperature to

1000 °C. N_2 adsorption measurements were carried out at −196 °C using a Belsorp 28SA automatic adsorption instrument (MicrotracBEL Corp., Osaka, Japan). The surface areas of the samples were obtained from a Brunauer–Emmett–Teller (BET) plot. Elemental analysis of Pd was measured by an inductive coupled plasma analysis, using a Thermo Jarrell Ash IRIS/AP instrument (SpectraLab Scientific Inc., Markham, ON, Canada).

3.4. Reactions

Before reaction, Pd/Mg(Al)O and Pd/C were reduced in a H_2 flow (60 mL/min) at 300 °C for 1 h. The reaction was carried out in a type of 100-mL stainless-steel autoclave reactor with a stirrer. In general, 0.2 g catalyst and 5 g hexadecyl palmitate ($C_{15}H_{31}COOC_{16}H_{33}$) were introduced into an autoclave reactor. Then, 0.9 MPa H_2 (for the reaction in H_2 atmosphere) or 0.9 MPa N_2 (for the reaction in N_2 atmosphere) was charged into the autoclave at room temperature (25 °C). The autoclave reactor was then heated and was kept at the reaction temperature (275–375 °C) for 1–6 h with vigorous stirring (600 rpm). After the reaction, the reactor was cooled down to room temperature before analysis.

3.5. Analyses

The gas products were collected into a plastic bag, from which the air had been taken out by using a pump. The total volume of the total gas was measured using a WS-1 integration flow meter (Shinagawa Corp., Tokyo, Japan). The composition of the gas products was analysed using gas chromatography (Shimadzu Corp., Kyoto, Japan). Inorganic gases (H_2, N_2, CO, and CO_2) were analysed using a Shimadzu 14B type GC with a thermal conductivity detector (TCD) that was equipped with MS-5A and Porapak-Q columns. Gaseous hydrocarbons (C_1–C_4) were analysed using a Shimadzu GC-2014 type FID-GC equipped with an RT-QPLOT (Agilent Technologies Japan, Ltd, Tokyo, Japan) capillary column. The factors of various gases (H_2, N_2, CO, CO_2, C_1–C_4 hydrocarbons) were obtained using a standard mixed gas (with known concentration for each component) from a cylinder.

The liquid products were taken out from the autoclave reactor. After filtering out the solid catalyst, a certain amount of dioxane ($C_4H_8O_2$) was added to the liquid products as an internal standard. Dichloromethane (CH_2Cl_2) was used as a solvent to wash the reactor and the used catalyst, and then mixed with the liquid products. The liquid products were analysed by a Shimadzu GC-2014 type GC-FID equipped with a UA-DX30 capillary column (Frontier Laboratories Ltd., Koriyama, Fukushima, Japan). Gas chromatography–mass spectrometry (GC-MS) analysis was performed on a Shimadzu GCMS-QP2010 Ultra (Shimadzu Corp., Kyoto, Japan) to confirm the components of the liquid products. Each component in the liquid product was separated on a UA-DX30 capillary column, and was identified by GC-MS analysis, with reference to the NIST-11 database. The amount of each normal paraffin in the product was calculated from the results of GC-FID analysis, and the factor of each normal paraffin was obtained using a pure reagent with a certain amount of dioxane ($C_4H_8O_2$) in the GC-FID analysis. Each olefin in the product was identified by GC-MS analysis, and the amount of each olefin was calculated from the results of GC-FID analysis by using the factor of a normal paraffin with the same number of carbon chains.

Using the results of the GC analyses, $C_{15}H_{31}COOC_{16}H_{33}$ conversion was calculated from the ratio of the decreased amount to the fed amount of $C_{15}H_{31}COOC_{16}H_{33}$; the yield of each carbon-containing product was calculated from the ratio of the formed amount of each product to the fed amount of $C_{15}H_{31}COOC_{16}H_{33}$. The carbon mass balance (before and after reaction) had an error less than ±5% for the reaction in H_2 atmosphere, and had an error less than ±10% for the reaction in N_2 atmosphere.

4. Conclusions

The Pd/Mg(Al)O catalyst derived from $Pd_{0.016}Mg_3Al(OH)_{16}CO_3{\cdot}xH_2O$ hydrotalcite precursor showed a high catalytic performance in both H_2 and N_2 atmospheres for the catalytic deoxygenation of $C_{15}H_{31}COOC_{16}H_{33}$. In H_2 atmosphere, the reduction of $C_{15}H_{31}COOC_{16}H_{33}$ was the main reaction, and the main products were n-$C_{16}H_{34}$ and n-$C_{15}H_{32}$ from the deoxygenation of $C_{15}H_{31}COOC_{16}H_{33}$

over Pd/Mg(Al)O. In N_2 atmosphere, the decarboxylation of $C_{15}H_{31}COOC_{16}H_{33}$ was the main reaction, and olefins and paraffins were formed as the products of deoxygenation of $C_{15}H_{31}COOC_{16}H_{33}$ over Pd/Mg(Al)O. The catalytic reaction in N_2 atmosphere was slower than that in H_2 atmosphere over Pd/Mg(Al)O. Pd/Mg(Al)O showed a much higher catalytic performance than that reported for other catalysts for the deoxygenation of $C_{15}H_{31}COOC_{16}H_{33}$ in N_2 atmosphere. Prolonging the reaction time or increasing the reaction temperature improved the yield of C_{10}–C_{16} hydrocarbons until the $C_{15}H_{31}COOC_{16}H_{33}$ conversion approached 100% for the reaction in N_2 atmosphere over the Pd/Mg(Al)O catalyst.

Author Contributions: The author Y.L. conceived and designed the experiments, Y.L. performed the experiments, Y.L, M.I., and K.M. analyzed the data, Y.L. drafted the paper. All authors have given approval for the final version of the manuscript.

Conflicts of Interest: The authors declare no conflict of interest.

References

1. Cesaro, A.; Belgiorno, V. Combined biogas and bioethanol production: Opportunities and challenge for industrial application. *Energies* **2015**, *8*, 8121–8144. [CrossRef]
2. Hanaoka, T.; Liu, Y.; Matsunaga, K.; Miyazawa, T.; Hirata, S.; Sakanishi, K. Bench-scale production of liquid fuel from woody biomass via gasification. *Fuel Process. Technol.* **2010**, *91*, 859–865. [CrossRef]
3. Liu, Y.; Hanaoka, T.; Miyazawa, T.; Murata, K.; Okabe, K.; Sakanishi, K. Fischer-Tropsch synthesis in slurry-phase reactors over Mn- and Zr-modified Co/SiO_2 catalysts. *Fuel Process. Technol.* **2009**, *90*, 901–908. [CrossRef]
4. Thanh, L.T.; Okitsu, K.; Boi, L.V.; Maeda, Y. Catalytic technologies for biodiesel fuel production and utilization of glycerol: A review. *Catalysts* **2012**, *2*, 191–222. [CrossRef]
5. Zhao, X.; Wei, L.; Cheng, S.; Julson, J. Review of heterogeneous catalysts for catalytically upgrading vegetable oils into hydrocarbon biofuels. *Catalysts* **2017**, *7*, 83. [CrossRef]
6. Liu, Y.; Sotelo-Boyas, R.; Murata, K.; Minowa, T.; Sakanishi, K. Production of bio-hydrogenated diesel by hydrotreatment of high-acid-value waste cooking oil over ruthenium catalyst supported on Al-polyoxocation-pillared pontmorillonite. *Catalysts* **2012**, *2*, 171–190. [CrossRef]
7. Liu, Y.; Sotelo-Boyas, R.; Murata, K.; Minowa, T.; Sakanishi, K. Hydrotreatment of vegetable oils to produce bio-hydrogenated diesel and liquefied petroleum gas fuel over catalysts containing sulfided Ni-Mo and solid Acids. *Energy Fuels* **2011**, *25*, 4675–4685. [CrossRef]
8. Yoshida, M.; Tanabe, Y.; Yonezawa, N.; Watanabe, M.M. Energy innovation potential of oleaginous microalgae. *Biofuels* **2012**, *3*, 761–781. [CrossRef]
9. Georgianna, D.R.; Mayfield, S.P. Exploiting diversity and synthetic biology for the production of algal biofuels. *Nature* **2012**, *488*, 329–335. [CrossRef] [PubMed]
10. Chisti, Y. Biodiesel from microalgae. *Biotechnol. Adv.* **2007**, *25*, 294–306. [CrossRef] [PubMed]
11. Milledge, J.J.; Smith, B.; Dyer, P.W.; Harvey, P. Macroalgae-derived biofuel: A review of method of energy extraction from seaweed biomass. *Energies* **2014**, *7*, 7194–7222. [CrossRef]
12. Kanda, H.; Li, P.; Goto, M.; Makio, H. Energy-saving lipid extraction from wet Euglena gracilis by the low-boiling-point solvent dimethyl ether. *Energies* **2015**, *8*, 610–620. [CrossRef]
13. Tani, Y.; Okumura, M.; Ii, S. Liquid wax ester production by euglena gracilis. *Agric. Biol. Chem.* **1987**, *51*, 225–230. [CrossRef]
14. Maki-Arvela, P.; Kubickova, I.; Snare, M.; Eranen, K.; Murzin, D.Y. Catalytic deoxygenation of fatty acids and their derivatives. *Energy Fuels* **2007**, *21*, 30–41. [CrossRef]
15. Sotelo-Boyas, R.; Liu, Y.; Minowa, T. Renewable diesel production from the hydrotreating of rapeseed oil with Pt/Zeolite and $NiMo/Al_2O_3$ catalysts. *Ind. Eng. Chem. Res.* **2011**, *50*, 2791–2799. [CrossRef]
16. Murata, K.; Liu, Y.; Watanabe, M.M.; Inaba, M.; Takahara, I. Hydrocracking of algae oil into aviation fuel-range hydrocarbons using a Pt-Re catalyst. *Energy Fuels* **2014**, *28*, 6999–7006. [CrossRef]
17. Sanchez-Cardenas, M.; Medina-Valtierra, J.; Kamaraj, S.-K.; Ramirez, R.R.M.; Sanchez-Olmos, L.A. Effect of size and distribution of Ni nanoparticles on γ-Al_2O_3 in oleic acid hydrodeoxygenation to produce *n*-alkanes. *Catalysts* **2016**, *6*, 156. [CrossRef]

18. Charusiri, W.; Vitidsant, T. Catalytic cracking of used cooking oil to liquid fuels over HZSM-5. *J. Energy* **2003**, *5*, 58–68.
19. Na, J.G.; Han, J.K.; Oh, Y.K.; Park, J.H.; Jung, T.S.; Han, S.S.; Yoon, H.C.; Chung, S.H.; Kim, J.N.; Ko, C.H. Decarboxylation of microalgal oil without hydrogen into hydrocarbon for the production of transportation fuel. *Catal. Today* **2012**, *185*, 313–317. [CrossRef]
20. Tani, H.; Hasegawa, T.; Shimouchi, M.; Asami, K.; Fujimoto, K. Selective catalytic decarboxy-cracking of triglyceride to middle-distillate hydrocarbon. *Catal. Today* **2011**, *164*, 410–414. [CrossRef]
21. Maki-Arvela, P.; Rozmyszowicz, B.; Lestari, S.; Simakova, O.; Eranen, K.; Salmi, T.; Murzin, D.Y. Catalytic deoxygenation of Tall oil fatty acid over palladium supported on mesoporous carbon. *Energy Fuels* **2011**, *25*, 2815–2825. [CrossRef]
22. Cavani, F.; Trifiro, F.; Vaccari, A. Hydrotalcite-type anionic clays: Preparation, properties and applications. *Catal. Today* **1991**, *11*, 173–301. [CrossRef]
23. Basile, F.; Basini, L.; Fornasari, G.; Gazzano, M.; Trifiro, F.; Vaccari, A. New hydrotalcite-type anionic clays containing noble metals. *Chem. Commun.* **1996**, 2435–2436. [CrossRef]
24. Narayanan, S.; Krishna, K. Structural influence of hydrotalcite on Pd dispersion and phenol hydrogenation. *Chem. Commun.* **1997**, 1991–1992. [CrossRef]
25. Basile, F.; Fornasari, G.; Gazzano, M.; Vaccari, A. Synthesis and thermal evolution of hydrotalcite-type compounds containing noble metals. *Appl. Clay Sci.* **2000**, *16*, 185–200. [CrossRef]
26. Davis, R.J.; Derouane, E.G. A non-porous supported-platinum catalyst for aromatization of *n*-hexane. *Nature* **1991**, *349*, 313–315. [CrossRef]
27. Liu, Y.; Murata, K.; Hanaoka, T.; Inaba, M.; Sakanishi, K. Syntheses of new peroxo-polyoxometalates intercalated layered double hydroxides for propene epoxidation by molecular oxygen in methanol. *J. Catal.* **2007**, *248*, 277–287. [CrossRef]
28. Liu, Y.; Murata, K.; Inaba, M. Direct epoxidation of proptlene by molecular oxygen over catalyst system containing palladium and peroxo-Heteropoly compound in methanol. *Chem. Commun.* **2004**, 582–583. [CrossRef] [PubMed]
29. Liu, Y.; Suzuki, K.; Hamakawa, S.; Hayakawa, T.; Murata, K.; Ishii, T.; Kumagai, M. Highly active methanol decomposition catalyst derived from Pd-hydrotalcite dispersed on mesoporous silica. *Catal. Lett.* **2000**, *66*, 205–213. [CrossRef]
30. Liu, Y.; Suzuki, K.; Hamakawa, S.; Hayakawa, T.; Murata, K.; Ishii, T.; Kumagai, M. Catalytic methanol decomposition at low temperature over Pd catalyst derived from mesoporous silica carried Pd-hydrotalcite. *Chem. Lett.* **2000**, 486–487. [CrossRef]
31. Liu, Y.; Suzuki, K.; Hayakawa, T.; Tsunoda, T.; Suzuki, K.; Hamakawa, S.; Murata, K.; Shiozaki, R.; Ishii, T.; Kumagai, M. Steam reforming of methanol over Cu/CeO_2 catalysts studied in comparison with Cu/ZnO and Cu/Zn(Al)O catalysts. *Top. Catal.* **2003**, *22*, 205–213. [CrossRef]
32. Liu, Y.; Hayakawa, T.; Suzuki, K.; Hamakawa, S.; Tsunoda, T.; Ishii, T.; Kumagai, M. High active copper/ceria catalysts for the steam reforming of methanol. *Appl. Catal. A Gen.* **2002**, *223*, 137–145. [CrossRef]
33. Liu, Y.; Hayakawa, T.; Ishii, T.; Kumagai, M.; Yasuda, H.; Suzuki, K.; Hamakawa, S.; Murata, K. Methanol decomposition to synthesis gas at low temperature over palladium support on ceria-zirconia solid solutions. *Appl. Catal. A Gen.* **2001**, *210*, 301–314. [CrossRef]
34. Liu, Y.; Murata, K.; Inaba, M.; Takahara, I.; Okabe, K. Mixed synthesis of mixed alcohols from syngas over Cs- and Ni-modified Cu/CeO_2 catalysts. *Fuel* **2013**, *104*, 62–69. [CrossRef]
35. Liu, Y.; Murata, K.; Inaba, M.; Takahara, I.; Okabe, K. Synthesis of ethanol from syngas over $Rh/Ce_{1-x}Zr_xO_2$ catalysts. *Catal. Today* **2011**, *164*, 308–314. [CrossRef]
36. Liu, Y.; Murata, K.; Sakanishi, K. Hydroisomerization-cracking of gasoline distillate from Fischer–Tropsch synthesis over bifunctional catalysts containing Pt and heteropolyacids. *Fuel* **2011**, *90*, 3056–3065. [CrossRef]
37. Liu, Y.; Sotelo-Boyás, R.; Murata, K.; Minowa, T.; Sakanishi, K. Hydrotreatment of Jatropha oil to produce green diesel over trifunctional Ni-Mo/SiO_2-Al_2O_3 catalyst. *Chem. Lett.* **2009**, *38*, 552–553. [CrossRef]
38. Liu, Y.; Koyano, G.; Misono, M. Hydroisomerization of *n*-hexane and *n*-heptane over platinum-promoted $Cs_{2.5}H_{0.5}PW_{12}O_{40}$ (Cs2.5) studied in comparison with several other solid acids. *Top. Catal.* **2000**, *11*, 239–246. [CrossRef]
39. Liu, Y.; Na, K.; Misono, M. Skeletal isomerization of *n*-pentane over Pt-promoted cesium hydrogen salts of 12-tungstophosphoric acid. *J. Mol. Catal. A Chem.* **1999**, *141*, 145–153. [CrossRef]

40. Liu, Y.; Misono, M. Hydroisomerization of *n*-butane over platinum-promoted cesium hydrogen salt of 12-tungstophosphoric acid. *Materials* **2009**, *2*, 2319–2336. [CrossRef]
41. Liu, Y.; Murata, K.; Okabe, K.; Inaba, M.; Takahara, I.; Hanaoka, T.; Sakanishi, K. Selective hydrocracking of Fischer-Tropsch waxes to high-quality diesel fuel over Pt-promoted polyoxocation-pillared montmorillonites. *Top. Catal.* **2009**, *52*, 597–608. [CrossRef]
42. Liu, Y.; Koyano, G.; Na, K.; Misono, M. Isomerization of *n*-pentane and *n*-hexane over cesium hydrogen salt of 12-tungstophosphoric acid promoted by platinum. *Appl. Catal. A Gen.* **1998**, *166*, L263–L265. [CrossRef]
43. Hattori, H. Heterogenous basic catalysis. *Chem. Rev.* **1995**, *95*, 537–558. [CrossRef]